

## Communication

**High Performance Nanostructured Supercapacitors on a Sponge**

Husam Niman Alshareef, Wei Chen, R B Rakhi, Liangbing Hu, Xing Xie, and Yi Cui

*Nano Lett.*, **Just Accepted Manuscript** • Publication Date (Web): 16 September 2011Downloaded from <http://pubs.acs.org> on September 18, 2011**Just Accepted**

“Just Accepted” manuscripts have been peer-reviewed and accepted for publication. They are posted online prior to technical editing, formatting for publication and author proofing. The American Chemical Society provides “Just Accepted” as a free service to the research community to expedite the dissemination of scientific material as soon as possible after acceptance. “Just Accepted” manuscripts appear in full in PDF format accompanied by an HTML abstract. “Just Accepted” manuscripts have been fully peer reviewed, but should not be considered the official version of record. They are accessible to all readers and citable by the Digital Object Identifier (DOI®). “Just Accepted” is an optional service offered to authors. Therefore, the “Just Accepted” Web site may not include all articles that will be published in the journal. After a manuscript is technically edited and formatted, it will be removed from the “Just Accepted” Web site and published as an ASAP article. Note that technical editing may introduce minor changes to the manuscript text and/or graphics which could affect content, and all legal disclaimers and ethical guidelines that apply to the journal pertain. ACS cannot be held responsible for errors or consequences arising from the use of information contained in these “Just Accepted” manuscripts.



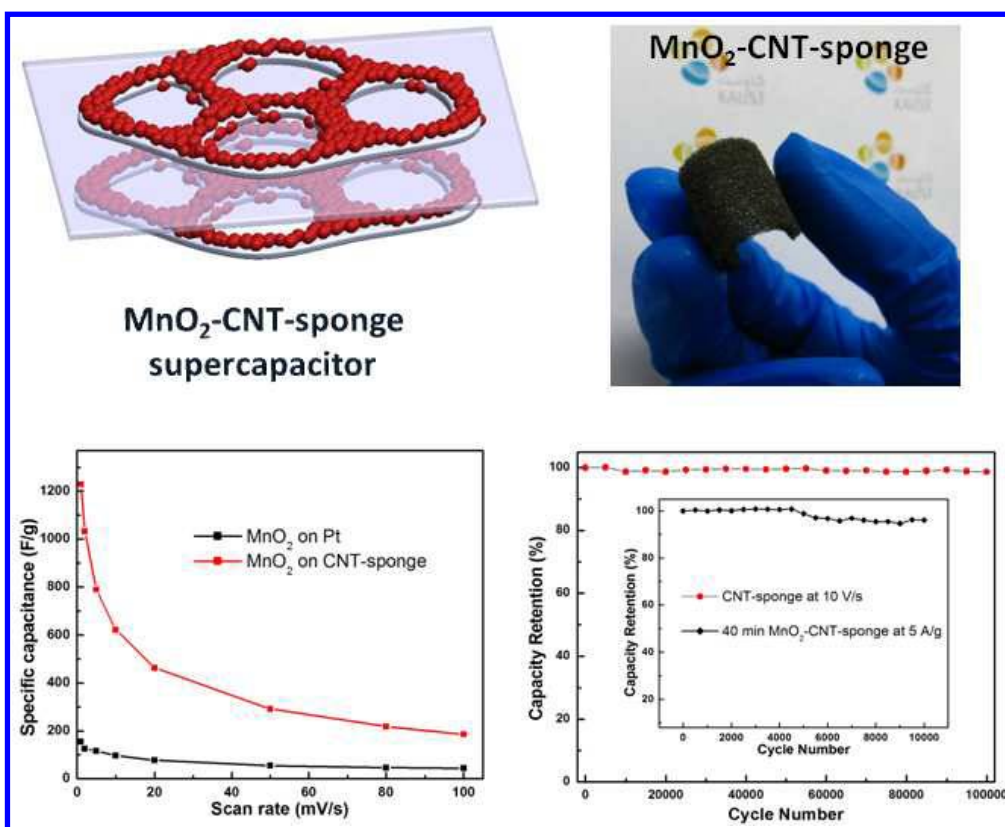
# High Performance Nanostructured Supercapacitors on a Sponge

Wei Chen<sup>1</sup>, R. B. Rakhi<sup>1</sup>, Liangbing Hu<sup>2</sup>, Xing Xie<sup>3</sup>, Yi Cui<sup>2</sup>, H. N. Alshareef<sup>\*,1</sup>

1 Materials Science and Engineering, King Abdullah University of Science and Technology (KAUST), Jeddah, Saudi Arabia 23955-6900; 2 Department of Materials Science and Engineering, Stanford University, California, USA 94305; 3 Department of Civil and Environmental Engineering, Stanford University, Stanford, California, USA 94305

\*To whom correspondence should be addressed, E-mail: [husam.alshareef@kaust.edu.sa](mailto:husam.alshareef@kaust.edu.sa)

## TABLE OF CONTENTS



\*Corresponding author: [husam.alshareef@kaust.edu.sa](mailto:husam.alshareef@kaust.edu.sa)

Phone: Office: +966-(0)2-808-4477 | Cell: +966-(0)5-44700037

ACS Paragon Plus Environment

**ABSTRACT**

A simple and scalable method has been developed to fabricate nanostructured MnO<sub>2</sub>-CNT-sponge hybrid electrodes. A novel supercapacitor, henceforth referred to as “sponge supercapacitor”, has been fabricated using these hybrid electrodes with remarkable performance. Ultrahigh specific capacitance (based on the mass of MnO<sub>2</sub>) of 1,230 F/g was achieved, which is close to the theoretical value of MnO<sub>2</sub>. Capacitors based on CNT-sponge substrates (without MnO<sub>2</sub>) can be operated even under an extremely high scan rate of 200 V/s, and they exhibit outstanding cycle performance with only 2% degradation after 100,000 cycles under a scan rate of 10 V/s. The MnO<sub>2</sub>-CNT-sponge supercapacitors show only 4% of degradation after 10,000 cycles at a charge-discharge specific current of 5 A/g. The specific power and energy of the MnO<sub>2</sub>-CNT-sponge supercapacitors are high with values of 63 kW/kg and 61 Wh/kg, respectively. The attractive performances exhibited by these sponge supercapacitors make them promising candidates for future high performance energy storage systems.

**KEYWORDS:** sponge supercapacitor, energy storage, specific capacitance, specific power, MnO<sub>2</sub>, carbon nanotubes.

1  
2  
3  
4  
5  
6  
7 Supercapacitors, also known as ultracapacitors, are promising energy storage devices that bridge the gap  
8 between batteries and conventional capacitors. Supercapacitors can provide higher energy density than  
9 conventional capacitors and much higher power density than batteries<sup>1-4</sup>. They exhibit a promising set of  
10 features such as high power density, fast rates of charge-discharge, reliable cycling life and safe  
11 operation<sup>1-5</sup>. Supercapacitors can be divided into two categories based on the underlying energy storage  
12 mechanism<sup>1,2,5</sup>. One is electrochemical double layer capacitor (EDLC), where electrical energy is stored  
13 by electrostatic accumulation of charges<sup>1</sup>. EDLC can provide ultrahigh power and excellent cycle life due  
14 to fast and non-degradation process between electrode active materials and electrolyte<sup>2</sup>. However, the  
15 energy stored in EDLCs is limited by the finite electrical charge separation at the interface of electrode  
16 materials and electrolyte and the availability of surface area<sup>4</sup>. Another type of supercapacitor is the so-  
17 called pseudocapacitor<sup>1-3,5</sup>, in which electrical energy is mainly stored by fast and reversible redox  
18 reactions. Because of the Faradaic process underpinning the energy stored in a pseudocapacitor, it has  
19 increased energy density but at the cost of power density and cycle life compared to EDLCs. Hybrid  
20 supercapacitors, combine these two charge storage mechanisms (Faradaic and non-Faradaic), resulting in  
21 improved device characteristics<sup>1,2,4,6-11</sup>. Typically, carbon based materials are good electrodes for  
22 EDLCs<sup>12-16</sup>, while transition metal oxides and electrically conducting polymers are good candidates for  
23 pseudocapacitors<sup>17-20</sup>. Among the different EDLC electrode materials, carbon nanotubes (CNTs) attracted  
24 the most attention due to their good conductivity, mechanical flexibility, and stable electrochemical  
25 behavior<sup>12,21-24</sup>. In comparison, MnO<sub>2</sub> is the most thoroughly investigated transition metal oxide for  
26 pseudocapacitors due to its high theoretical specific capacitance (1370 F/g)<sup>25</sup>, relatively low cost, and  
27 environmental friendliness<sup>17,26</sup>. However, the theoretical capacitance of MnO<sub>2</sub> has rarely been achieved in  
28 experiment<sup>25</sup>, mainly due to its poor electrical conductivity (10<sup>-5</sup> – 10<sup>-6</sup> S/cm). In order to get high specific  
29 capacitance from MnO<sub>2</sub>, many studies have been conducted, most of which are based on incorporating  
30 MnO<sub>2</sub> with conductive materials and forming hybrid electrode structures.<sup>7,8,26-28</sup> Several examples of  
31  
32  
33  
34  
35  
36  
37  
38  
39  
40  
41  
42  
43  
44  
45  
46  
47  
48  
49  
50  
51  
52  
53  
54  
55  
56  
57  
58  
59  
60

1  
2  
3 MnO<sub>2</sub> based hybrid electrodes have been recently demonstrated. Hou *et al.* synthesized a  
4 MnO<sub>2</sub>/CNT/conducting polymer ternary electrodes with a specific capacitance of 427 F/g (based on three-  
5 electrode setup)<sup>29</sup>. Bao *et al.* demonstrated flexible supercapacitors using Zn<sub>2</sub>SnO<sub>4</sub>/MnO<sub>2</sub> core/shell  
6 nanocable coated on carbon microfiber with a specific capacitance of 642.4 F/g (based on three-electrode  
7 setup)<sup>30</sup>. Very recently, Lang *et al.* developed a supercapacitor based on nanoporous gold and MnO<sub>2</sub>, with  
8 a high specific capacitance of 1,145 F/g (based on two-electrode setup), which is close to the theoretical  
9 value<sup>31</sup>. However, these fabrication processes are either too complicated or limited in scalability.  
10 Previously, we have exploited paper and textile as substrates to fabricate supercapacitors since they  
11 provide highly porous structure for the fast access of ions to electrolytes<sup>32-35</sup>. Different from the paper and  
12 textile in the previous work, here we exploited sponge as the substrate for supercapacitors.  
13  
14  
15  
16  
17  
18  
19  
20  
21  
22  
23  
24

25  
26 Sponges, with a hierarchical macroporous nature, have been widely used in our daily life as cleaning tools  
27 and can be found everywhere. Sponges are made up of many small cellulose or polyester fibers, which  
28 make them highly porous and strong absorbing media with significant internal surface area. A  
29 commercial sponge has been employed into our work, which has a high water absorption capacity. A  
30 simple experiment showed that it can absorb 45 times more water than its own weight. This indicates the  
31 good accessibility and compatibility of sponge to water and aqueous solutions. Sponges offer novel  
32 exciting characteristics different from paper and textile: first, Sponge has much more uniform size of  
33 macropores. The pore size can be in the range of 100-500 μm. Second, the cellulose or polyester fibers  
34 are interconnect virtually free of junctions. Therefore, continuous coating of conducting nanomaterials is  
35 much easier since there are no junctions to cross.  
36  
37  
38  
39  
40  
41  
42  
43  
44  
45  
46  
47

48 We have designed and fabricated high performance supercapacitors using a simple and scalable method.  
49 The fabrication process consisted of four simple steps, as illustrated in Figure 1. A piece of commercially  
50 available sponge (pore sizes 100-500 μm) was cleaned by water and acetone for several times (Fig.1 (a)).  
51 After drying completely in a vacuum oven, the sponge was cut into small ribbons with thickness of 1 mm  
52 and area of 1×2 cm<sup>2</sup>. The sponge ribbons were subsequently coated with CNTs using a simple “dipping  
53  
54  
55  
56  
57  
58  
59  
60

1  
2  
3 and drying” process in CNT ink suspension (Fig.1 (b)) (for details, see Supporting Information). The  
4  
5 next step was to electrodeposit  $\text{MnO}_2$  nanoparticles on the CNT-coated sponge by galvanostatic  
6  
7 electrochemical deposition (Fig.1 (c)). A very small current density ( $500 \mu\text{A}/\text{cm}^2$ ) was required to obtain  
8  
9 the desired nanostructure of  $\text{MnO}_2$ . To study the dependence of supercapacitor performance on  $\text{MnO}_2$   
10  
11 deposition time, we deposited  $\text{MnO}_2$  on CNT-sponge for different times: ranging from 3 minutes to 40  
12  
13 minutes. The deposition area of each sample was  $1 \times 1 \text{ cm}^2$ . In the last step (Fig.1 (d)), two identical  
14  
15  $\text{MnO}_2$ -CNT-sponges were sandwiched with a piece of polymer separator dipped in 1 M  $\text{Na}_2\text{SO}_4$   
16  
17 electrolyte inserted in between, and sealed in a coin cell to complete the symmetrical two electrode  
18  
19 assembly (for details, see Supporting Information).  
20  
21  
22

23  
24 The weight of a clean  $1 \times 2 \text{ cm}^2$  sponge was about 10 mg, which is much lighter than the rigid metal and  
25  
26 other flexible substrates with the same area<sup>36-38</sup>. Due to the mechanical flexibility of CNTs and strong van  
27  
28 der Waals interactions between the macroporous sponge cellulose and CNTs, the CNTs can be easily  
29  
30 coated onto the skeleton of a sponge, rendering the insulating sponge highly conductive by a simple  
31  
32 dipping and drying process.<sup>33</sup> The CNT-sponge has a sheet resistance of 1 Ohm/square, measured by four  
33  
34 points probe technique. After conformal coating of CNTs onto the skeleton of the sponge, it still  
35  
36 maintained hierarchical macroporous nature where its intricate assembly of pores remained open to allow  
37  
38 the flow of electrolyte (Supporting Fig. 1S-a). The CNTs coated on the sponge have formed a thin layer  
39  
40 of CNT network wrapped around the skeleton of sponge (Supporting Fig. 1S-b, c). The amount of CNTs  
41  
42 coating on sponge can be readily controlled by the dipping time and ink concentration. In this work, we  
43  
44 optimized the dipping time to maximize the amount of CNTs coated on the sponge without blocking its  
45  
46 pores. Undercoating degrades the conductivity of the CNT-sponge electrode while overcoating closes the  
47  
48 pores of the sponge and prevents the movement of the electrolyte ions. The mechanical resilience of the  
49  
50 CNT-sponge skeleton was tested by folding, twisting, and stretching it repeatedly as shown in Supporting  
51  
52 Fig. 4S-d, e, f. After all the mechanical tests, the CNT-sponge always reverted to its original shape  
53  
54 without any permanent deformation.  
55  
56  
57  
58  
59  
60

SEM images of MnO<sub>2</sub>-CNT-sponge showed clearly the three-dimensional (3D) hierarchical macroporous open-pore structure (Fig. 2a, Supporting Fig. 2S-a). Flower-like MnO<sub>2</sub> nanoparticles were uniformly deposited onto the conductive CNT-sponge skeleton, even at the edges (Fig. 2b, c, Supporting Fig. 2S-b, c). This further confirms that CNTs have been conformably coated on the sponge. Fig. 2a also shows an exciting point: the backbone of sponge is free of junctions and promotes the continuous coating of CNT to form excellent conducting pathways in the whole structure. After deposition of MnO<sub>2</sub>, the highly porous nanostructure remained, which is good for the fast transportation of electrons and ions in the supercapacitor devices. The deposition mass of MnO<sub>2</sub> can be well controlled by adjusting the deposition time (Supporting Fig. 3S). We found that the surface of the CNT-sponge can be fully covered by MnO<sub>2</sub> after 10-minute electrodeposition (Supporting Fig. 3S-c). Increasing the deposition time will increase the mass loading and the thickness of MnO<sub>2</sub>, as shown in the supporting information Fig. 3S. If the electrodeposition is run for one hour, a very thick film of MnO<sub>2</sub> with some cracks can be observed due to the large thickness (Supporting Fig. 3S-f). TEM images revealed that the nanostructure of MnO<sub>2</sub> is highly porous and includes many small nanoplates (Fig. 2d, Supporting Fig. 2S-d). The average pore size of the MnO<sub>2</sub> is around 3.2 nm and it has a BET specific surface area of 174 m<sup>2</sup>/g (Supporting Fig. 4S). An HRTEM image together with selected area electron diffraction (SAED) pattern demonstrated that the deposited MnO<sub>2</sub> are polycrystalline (Fig. 2e and inset, Supporting Fig. 2S-e). We further confirmed that the polycrystalline MnO<sub>2</sub> nanoparticles belong to ε-MnO<sub>2</sub> by XRD (JCPDS 00-030-0820) (Fig. 2f). The flower-like MnO<sub>2</sub> nanoparticles on macroporous CNT-sponge essentially form a so-called double porous nanostructure<sup>33</sup>. This unique structure provides outstanding performance for the intercalation/deintercalation of electrolyte cations into electrode materials, and we therefore expect a high performance supercapacitor.

The electrochemical performance of CNT-sponge substrate was tested using a two-electrode coin cell configuration. Two pieces of symmetrical CNT-sponge, one piece of separator and 1 M Na<sub>2</sub>SO<sub>4</sub> have been used as electrodes, separator and electrolyte, respectively. All measurements have been conducted at

1  
2  
3 room temperature. As shown in Fig. 3a and b, the CNT-sponge devices (without MnO<sub>2</sub> deposition) can be  
4 operated over a wide range of scan rates: from 1 mV/s up to 200 V/s. The cyclic voltammograms retain  
5 the rectangular shape (which is characteristic of the ideal electrochemical double layer capacitive  
6 behavior) even at a high scan rate of 20 V/s. As expected, the currents increase with the applied scan rates,  
7 but surprisingly the CNT-sponge devices operates at the highest reported scan rate for aqueous electrolyte  
8 supercapacitors<sup>7,25,28,35-38</sup>. We can therefore conclude that ultrahigh power can be obtained from this kind of  
9 device<sup>14</sup>. Another good feature of the CNT-sponge device is its good electrochemical behavior even at an  
10 extremely high scan rate of 200 V/s, which is comparable to micro-supercapacitors built on rigid silicone  
11 substrates<sup>14,16,39</sup>. Furthermore, a linear dependence of the discharge current on the scan rate up to 8 V/s  
12 can be observed from Fig. 3c. The deviation of the linear dependence after 8 V/s is due to the diffusion  
13 limit of electrolyte ions to the electrode materials. The discharge currents are calculated from the  
14 discharge scan with an average over the whole voltage range at specific scan rates<sup>14,39</sup>. A mean areal  
15 capacitance of 0.36 mF/cm<sup>2</sup> can be obtained from the slope of Fig. 3c, which is comparable to the value  
16 of carbon materials based micro-supercapacitors<sup>39</sup>. A maximal value of 0.9 mF/cm<sup>2</sup> can also be obtained  
17 at a scan rate of 1 mV/s, but this value can be improved if more CNTs have been coated on the sponge.  
18 Fig. 3d illustrated the charge-discharge behavior of the CNT-sponge device. The figure shows ultrafast  
19 charge-discharge rate and linear dependence on voltage and time, with very small voltage drop at a  
20 specific current of 10 A/g. These results indicate that the CNT-sponge substrates used in the present work  
21 exhibit excellent supercapacitor performance. More importantly, these results coupled with other  
22 promising features of the CNT-sponge (such as ease of fabrication, low cost, light weight and flexibility)  
23 make it a highly promising energy storage substrate.  
24  
25  
26  
27  
28  
29  
30  
31  
32  
33  
34  
35  
36  
37  
38  
39  
40  
41  
42  
43  
44  
45  
46  
47  
48

49 Fig. 4e shows the MnO<sub>2</sub>-CNT-sponge electrodes prepared by electrochemical deposition of MnO<sub>2</sub> onto  
50 conductive CNT-sponge. The amount of MnO<sub>2</sub> was controlled by the deposition time. Here, we varied the  
51 deposition time from 3 minutes to 40 minutes. It was observed that as the deposition time increased, the  
52 mass loading of MnO<sub>2</sub> increased accordingly. This can be observed from the increased darkness of the  
53  
54  
55  
56  
57  
58  
59  
60



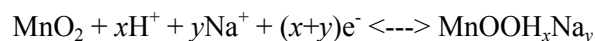
1  
2  
3 sponge as shown in Fig. 4b. The first ribbon on the left in Fig. 4b is a bare sponge, and the second one  
4  
5 from the left is a CNT-sponge without MnO<sub>2</sub> on it. The remaining samples from left to right are MnO<sub>2</sub>-  
6  
7 CNT-sponge with deposition time from 3 minutes to 40 minutes. The color of the bottom part of the  
8  
9 CNT-sponge becomes darker with increased electrodeposition time, which means more MnO<sub>2</sub> has been  
10  
11 deposited on the sponge. This can be further confirmed by plotting the change of MnO<sub>2</sub> content and  
12  
13 MnO<sub>2</sub> mass loading versus deposition time (Fig. 4a). As can be seen from Fig. 4a, the MnO<sub>2</sub> content (the  
14  
15 weight percentage of MnO<sub>2</sub> in MnO<sub>2</sub>-CNT composite) and its mass loading increased with the deposition  
16  
17 time. Each data point in Fig. 4a is an average value of at least 10 samples. At low deposition time, e.g., 10  
18  
19 minute, the MnO<sub>2</sub> mass loading is around 0.1 mg/cm<sup>2</sup> and its content in the MnO<sub>2</sub>-CNT composite is  
20  
21 nearly 30% by weight. These values are higher than the values obtained from rigid metal substrates such  
22  
23 as platinum at the same deposition time due to the large surface area of the sponge. When the  
24  
25 electrodeposition time increased to 40 minutes, the mass loading of MnO<sub>2</sub> increased to 0.5 mg/cm<sup>2</sup>, which  
26  
27 is more than twice of CNT loading on the sponge, and the corresponding MnO<sub>2</sub> content in the MnO<sub>2</sub>-CNT  
28  
29 composite is as high as 67% by weight. For long deposition times, e.g. 20 hours, the mass loading of  
30  
31 MnO<sub>2</sub> can go up to 12.8 mg/cm<sup>2</sup>, which is twice of the weight than the CNT-sponge itself. To reveal the  
32  
33 good adhesion between MnO<sub>2</sub> and CNT-sponge, a simple Scotch tape adhesion test was performed  
34  
35 comparing the MnO<sub>2</sub>-CNT-sponge and MnO<sub>2</sub>-platinum electrodes. It can be seen clearly from Fig. 4c that  
36  
37 superior adhesion performance is observed for the MnO<sub>2</sub>-CNT-sponge: no peeling was observed in the  
38  
39 case of MnO<sub>2</sub>-CNT-sponge, while significant peeling was observed in the case of the rigid Pt foil (Fig.  
40  
41 4d). Another result that demonstrates the superior electrochemical performance of the MnO<sub>2</sub>-CNT-sponge  
42  
43 electrodes is comparing its cyclic voltammetry behavior to the flat MnO<sub>2</sub>-Pt substrate. A three-electrode  
44  
45 configuration has been setup to test the electrochemical performances by cyclic voltammogram (for  
46  
47 details, see Supporting Information). At scan rate of 50 mV/s (Fig. 4f), the electrochemical performance  
48  
49 of MnO<sub>2</sub>-CNT-sponge outperforms that of MnO<sub>2</sub>-Pt electrode in terms of wider voltage range and higher  
50  
51 capacitance. At a five-minute electrodeposition of MnO<sub>2</sub>, a very high specific capacitance of 1,230 F/g  
52  
53 can be achieved from MnO<sub>2</sub>-CNT-sponge electrode at scan rate of 1 mV/s. However, the value is just 155  
54  
55  
56  
57  
58  
59  
60

1  
2  
3 F/g for MnO<sub>2</sub>-Pt electrode under the same condition (Fig. 4g). This controlled experiment further  
4 confirms the outstanding electrochemical performance of MnO<sub>2</sub>-CNT-sponge electrode.  
5  
6

7  
8 To completely investigate the electrochemical performances of MnO<sub>2</sub>-CNT-sponge supercapacitors, a  
9 typical two-electrode configuration has been employed in this work<sup>40,41</sup>. The MnO<sub>2</sub>-CNT-sponge serves as  
10 electrode as well as current collector, and the integrated binder-free structure provides highly porous and  
11 conductive channels for the full access of electrolyte ions to the active electrode material in  
12 supercapacitors. As shown in Fig. 5a and b, the full cell has been studied by cyclic voltammograms over a  
13 wide range of scan rates: from 1 mV/s to 10 V/s. All samples behaved like ideal EDLCs at scan rates up  
14 to 1500 mV/s. Take the 5 minute MnO<sub>2</sub> deposition sample as an example. The CV shapes are almost  
15 rectangular at scan rates below 2 V/s and remain quasi-rectangular at scan rate up to 10 V/s, indicating the  
16 excellent charge storage characteristics and ultrafast response of the electrodes. The high scan rate of 10  
17 V/s is two orders of magnitude higher than the rate used in most of the literature for the MnO<sub>2</sub>/CNT  
18 composite electrodes with aqueous electrolyte<sup>7,8,28-30</sup>. The voltages versus time profiles were obtained by  
19 galvanostatic charge-discharge measurements (Fig. 5c). The device can be steadily operated over a wide  
20 range of applied specific current, from 1 A/g to 100 A/g. The internal resistances<sup>41,42</sup> (including the  
21 electrical resistances of electrodes, the ions diffusion resistances and the interfacial resistance between the  
22 electrode and electrolyte) derived from the voltage drop are consistent with the values calculated from  
23 impedance electrochemical spectroscopy (Supporting Fig. 5S). The cyclic voltammetry response of  
24 different samples under different deposition times have been demonstrated in Fig. 5d and e, at specific  
25 scan rate of 20 mV/s and 200 mV/s, respectively. The corresponding current increases with MnO<sub>2</sub> content  
26 on the electrodes for both scan rates, suggesting that more materials contributed to charge storage. When  
27 the scan rate changed from 20 mV/s to 200 mV/s, the CV shapes remained nearly rectangular, with only a  
28 few deviations for samples with high mass loading. This clearly shows the excellent electrochemical  
29 performance of the MnO<sub>2</sub>-CNT-sponge supercapacitors. The specific capacitances with respect to the  
30 mass of MnO<sub>2</sub> have been derived from CVs and plotted in Fig. 5f, which are comparable with the values  
31  
32  
33  
34  
35  
36  
37  
38  
39  
40  
41  
42  
43  
44  
45  
46  
47  
48  
49  
50  
51  
52  
53  
54  
55  
56  
57  
58  
59  
60

1  
2  
3 calculated from galvanostatic charge-discharge curves. A specific capacitance of 1,000 F/g can be readily  
4  
5 obtained based on the mass of MnO<sub>2</sub> at scan rate of 1 mV/s. The specific capacitances of MnO<sub>2</sub>-CNT-  
6  
7 sponge supercapacitor are one to two orders higher than that of CNT-sponge device, indicating the  
8  
9 significant contribution from porous MnO<sub>2</sub>, and these values are much higher than that from  
10  
11 literature<sup>29,30,35-38,43</sup>. The specific capacitance decreases with the scan rates and MnO<sub>2</sub> deposition times, but  
12  
13 remains constant at scan rates higher than 100 mV/s. The measured specific capacitance depends strongly  
14  
15 on scan rate for low mass loading devices, but depends weakly on scan rate for high mass loading devices.  
16  
17 For example, the specific capacitance decreased from 1,000 F/g at 1 mV/s to 581 F/g at 100 mV/s for the  
18  
19 three-minute electrodeposition device. In comparison, it decreased from 444 F/g at 1 mV/s to 295 F/g at  
20  
21 100 mV/s for the ten-minute electrodeposition device. For higher mass loading devices, such as 30  
22  
23 minutes and 40 minutes MnO<sub>2</sub> depositions, negligible change in specific capacitance was observed,  
24  
25 especially at high scan rates. This is mainly due to the limited conductivity of high mass loading samples  
26  
27 and the limited utilization of MnO<sub>2</sub> at high scan rates. At low mass loading of MnO<sub>2</sub>, the highly  
28  
29 conductive double porous electrodes provide good opportunity for electron transportation and ions  
30  
31 accessibility, maximizing the utilization of MnO<sub>2</sub> materials. At even lower deposition time, the theoretical  
32  
33 specific capacitance can be practically achieved in this unique structure.  
34  
35  
36  
37  
38

39 Looking into the charge storage mechanisms<sup>2</sup> of MnO<sub>2</sub>-CNT-sponge supercapacitors, a possible  
40  
41 electrochemical reaction can be proposed as the following:  
42  
43



44  
45  
46 The energy storage contributions come from both surface adsorption/desorption of electrolyte cations  
47  
48 (Na<sup>+</sup>) to the surface of CNTs and MnO<sub>2</sub>, and the fast, reversible redox reactions by means of  
49  
50 intercalation/extraction of protons into/out of MnO<sub>2</sub>.<sup>2,31</sup> The conductive double porous structure facilitates  
51  
52 the adsorption/desorption of Na<sup>+</sup> and the transportation of electrons and protons, allowing full access of  
53  
54 the electrolyte to electrode materials and maximizing the utilization of MnO<sub>2</sub>. Therefore, the cyclic  
55  
56  
57  
58  
59  
60

1  
2  
3 voltammograms exhibit the ideal rectangular shapes and a very high specific capacitance of 1,000 F/g can  
4  
5 be readily obtained based on the mass of MnO<sub>2</sub>.  
6  
7

8  
9 Electrochemical impedance spectroscopy (EIS) and long time cycling stability are two important  
10 parameters to determine the performances of supercapacitors. Fig. 6a and inset show the Nyquist plots in  
11 the frequency range from 100 kHz to 0.01 Hz, which can be represented by the equivalent circuit and the  
12 corresponding model for ideal supercapacitors, as shown in Fig. 6b (ref. 1, 7, 30). In the equivalent circuit,  
13 a solution resistance ( $R_s$ ) connects in series with a constant phase element (CPE), and the CPE connects  
14 in parallel with the charge transfer resistance ( $R_{CT}$ ) and pseudo-capacitance ( $C_p$ ). The solution resistance  
15 refers to the resistance from the electrolyte, the CPE accounts for the double-layer capacitance, and the  
16 charge transfer resistance (also called Faraday resistance) corresponds to the total resistance at the  
17 interface between the electrode and the electrolyte<sup>44</sup>. Experimental results show that  $R_s$  is insensitive to  
18 the surface condition of the electrode, and it is consistent with a value of around 1.5  $\Omega$  for all our devices.  
19  
20 However,  $R_{CT}$  increases with the mass loading of MnO<sub>2</sub> on the surface of the CNT-sponge, from 4.5  $\Omega$  at  
21 3-min MnO<sub>2</sub> electrodeposition to 28  $\Omega$  at 40-min deposition (Fig. 6a). Typically, the Nyquist plot can be  
22 divided by the so-called knee frequency into a high frequency semicircle and a low frequency vertical  
23 line<sup>44</sup>, as schematically illustrated in Fig. 6b. The semi-circle intersection with the abscissa depends on the  
24 internal resistance and the vertical line implies good capacitive behaviors of supercapacitors. The internal  
25 resistances (including  $R_s$ ,  $R_{CT}$  and other resistances) of all samples are summarized and plotted in  
26 Supporting Fig. 5S. These values are consistent with those derived from the voltage drop of charge-  
27 discharge curves. This result clearly indicates that the internal resistance increases with the MnO<sub>2</sub>  
28 deposition time due to increased mass loading of semiconducting MnO<sub>2</sub>, making the MnO<sub>2</sub>-CNT-sponge  
29 electrode less conductive. A long time charge-discharge cycling up to 100,000 cycles has been performed  
30 on CNT-sponge devices using a scan rate of 10 V/s. The results, shown in Fig. 6c, indicate that 98% of  
31 the initial capacitance is retained. In comparison, the cycling stability of MnO<sub>2</sub>-CNT-sponge  
32 supercapacitors was also investigated up to 10,000 charge-discharge cycles using a specific current of 5  
33  
34  
35  
36  
37  
38  
39  
40  
41  
42  
43  
44  
45  
46  
47  
48  
49  
50  
51  
52  
53  
54  
55  
56  
57  
58  
59  
60

1  
2  
3 A/g. It is seen that 96% of the initial capacitance has been retained after 10,000 cycles (Fig. 6c inset) for  
4 the 40-minute MnO<sub>2</sub> deposition device. These results demonstrate good stability of both CNT-sponge and  
5 MnO<sub>2</sub>-CNT-sponge supercapacitors. Fig. 6d shows a Ragone plot of MnO<sub>2</sub>-CNT-sponge supercapacitors.  
6  
7 The Ragone plot shows that the specific energy and specific power values of our sponge supercapacitors  
8 are higher than the ones reported in the literature<sup>22,27,30,31,43,45,46</sup>, with maximum specific energy of 61  
9 Wh/kg and specific power of 63 kW/kg. The CNT-sponge device showed ultrahigh specific power of 105  
10 kW/kg, although the specific energy is low. All the specific energy and power values were calculated  
11 from the galvanostatic charge-discharge curves. These values demonstrate the outstanding capability of  
12 CNT-sponge and MnO<sub>2</sub>-CNT-sponge supercapacitors as high power and high energy storage systems.  
13  
14  
15  
16  
17  
18  
19  
20  
21  
22

23  
24 In summary, novel sponge supercapacitors have been fabricated using a simple method while providing  
25 remarkable performance. The macroporous nature of the sponge along with the porous nature of the  
26 electrodeposited MnO<sub>2</sub> nanoparticles provided a double porous electrode structure giving good  
27 conductivity and full accessibility of electrolyte to MnO<sub>2</sub>, improving the performances of MnO<sub>2</sub>-CNT-  
28 sponge supercapacitors dramatically. The MnO<sub>2</sub>-CNT-sponge supercapacitor exhibits very high specific  
29 capacitance, ultra fast charge-discharge rate, excellent cycling stability as well as good energy and power  
30 density, making it one of the most promising electrodes for high performance large-scale energy storage  
31 systems.  
32  
33  
34  
35  
36  
37  
38  
39  
40  
41  
42  
43  
44  
45  
46  
47  
48  
49  
50  
51

## 52 **Supporting Information.**

53  
54  
55  
56 Materials and Methods and additional supporting figures. This material is available free of charge via the  
57 Internet at <http://pubs.acs.org>  
58  
59  
60

**ACKNOWLEDGEMENT**

The authors thank for the characterization analysis provided by KAUST Advanced Imaging and Characterization Laboratory and Analytic Core Laboratory. W.C. acknowledges support from KAUST discovery fellowship. H.A. acknowledges the support from KAUST baseline fund. Y.C. acknowledges support from the King Abdullah University of Science and Technology (KAUST) Investigator Award (No. KUS-11-001-12) and the Precourt Institute for Energy at Stanford. X.X. acknowledges support from the Stanford Graduate Fellowship.

## References

- (1) Conway, B. E. *Electrochemical Supercapacitors: Scientific Fundamentals and Technological Applications*; Kluwer Academic/Plenum: New York, 1999.
- (2) Simon, P.; Gogotsi, Y. *Nature Materials* **2008**, *7*, 845.
- (3) Winter, M.; Brodd, R. J. *Chemical Reviews* **2005**, *105*, 1021.
- (4) Zhang, L. L.; Zhao, X. S. *Chemical Society Reviews* **2009**, *38*, 2520.
- (5) Arico, A. S.; Bruce, P.; Scrosati, B.; Tarascon, J. M.; Van Schalkwijk, W. *Nature Materials* **2005**, *4*, 366.
- (6) Chen, Z.; Augustyn, V.; Wen, J.; Zhang, Y. W.; Shen, M. Q.; Dunn, B.; Lu, Y. F. *Advanced Materials* **2011**, *23*, 791.
- (7) Liu, J. W.; Essner, J.; Li, J. *Chemistry of Materials* **2010**, *22*, 5022.
- (8) Reddy, A. L. M.; Shaijumon, M. M.; Gowda, S. R.; Ajayan, P. M. *Journal of Physical Chemistry C* **2010**, *114*, 658.
- (9) Mai, L.-Q.; Yang, F.; Zhao, Y.-L.; Xu, X.; Xu, L.; Luo, Y.-Z. *Nat Commun* **2011**, *2*, 381.
- (10) Rakhi, R. B.; Cha, D.; Chen, W.; Alshareef, H. N. *The Journal of Physical Chemistry C* **2011**, *115*, 14392.
- (11) Chen, S.; Zhu, J.; Wu, X.; Han, Q.; Wang, X. *ACS Nano* **2010**, *4*, 2822.
- (12) Frackowiak, E.; Beguin, F. *Carbon* **2001**, *39*, 937.
- (13) Chmiola, J.; Largeot, C.; Taberna, P. L.; Simon, P.; Gogotsi, Y. *Science* **2010**, *328*, 480.
- (14) Pech, D.; Brunet, M.; Durou, H.; Huang, P. H.; Mochalin, V.; Gogotsi, Y.; Taberna, P. L.; Simon, P. *Nature Nanotechnology* **2010**, *5*, 651.
- (15) Stoller, M. D.; Park, S. J.; Zhu, Y. W.; An, J. H.; Ruoff, R. S. *Nano Letters* **2008**, *8*, 3498.
- (16) Gao, W.; Singh, N.; Song, L.; Liu, Z.; Reddy, A. L. M.; Ci, L.; Vajtai, R.; Zhang, Q.; Wei, B.; Ajayan, P. M. *Nat Nano* **2011**, *6*, 496.
- (17) Lee, H. Y.; Goodenough, J. B. *Journal of Solid State Chemistry* **1999**, *144*, 220.
- (18) Hu, C. C.; Tsou, T. W. *Electrochemistry Communications* **2002**, *4*, 105.
- (19) Wang, Y. G.; Li, H. Q.; Xia, Y. Y. *Advanced Materials* **2006**, *18*, 2619.
- (20) Rakhi, R. B.; Alshareef, H. N. *Journal of Power Sources* **2011**, *196*, 8858.
- (21) Futaba, D. N.; Hata, K.; Yamada, T.; Hiraoka, T.; Hayamizu, Y.; Kakudate, Y.; Tanaike, O.; Hatori, H.; Yumura, M.; Iijima, S. *Nature Materials* **2006**, *5*, 987.
- (22) An, K. H.; Kim, W. S.; Park, Y. S.; Moon, J. M.; Bae, D. J.; Lim, S. C.; Lee, Y. S.; Lee, Y. H. *Advanced Functional Materials* **2001**, *11*, 387.
- (23) Pushparaj, V. L.; Shaijumon, M. M.; Kumar, A.; Murugesan, S.; Ci, L.; Vajtai, R.; Linhardt, R. J.; Nalamasu, O.; Ajayan, P. M. *Proceedings of the National Academy of Sciences of the United States of America* **2007**, *104*, 13574.
- (24) Kaempgen, M.; Chan, C. K.; Ma, J.; Cui, Y.; Gruner, G. *Nano Letters* **2009**, *9*, 1872.
- (25) Toupin, M.; Brousse, T.; Belanger, D. *Chemistry of Materials* **2004**, *16*, 3184.
- (26) Wei, W. F.; Cui, X. W.; Chen, W. X.; Ivey, D. G. *Chemical Society Reviews* **2011**, *40*, 1697.
- (27) Wu, Z. S.; Ren, W. C.; Wang, D. W.; Li, F.; Liu, B. L.; Cheng, H. M. *Acs Nano* **2010**, *4*, 5835.
- (28) Lee, S. W.; Kim, J.; Chen, S.; Hammond, P. T.; Shao-Horn, Y. *Acs Nano* **2010**, *4*, 3889.
- (29) Hou, Y.; Cheng, Y. W.; Hobson, T.; Liu, J. *Nano Letters* **2010**, *10*, 2727.
- (30) Bao, L. H.; Zang, J. F.; Li, X. D. *Nano Letters* **2011**, *11*, 1215.
- (31) Lang, X. Y.; Hirata, A.; Fujita, T.; Chen, M. W. *Nature Nanotechnology* **2011**, *6*, 232.
- (32) Hu, L.; Choi, J. W.; Yang, Y.; Jeong, S.; La Mantia, F.; Cui, L.-F.; Cui, Y. *Proceedings of the National Academy of Sciences* **2009**, *106*, 21490.
- (33) Hu, L.; Pasta, M.; Mantia, F. L.; Cui, L.; Jeong, S.; Deshazer, H. D.; Choi, J. W.; Han, S. M.; Cui, Y. *Nano Letters* **2010**, *10*, 708.

- 1  
2  
3 (34) Pasta, M.; La Mantia, F.; Hu, L.; Deshazer, H.; Cui, Y. *Nano Research* **2010**, *3*, 452.  
4 (35) Yu, G.; Hu, L.; Vosgueritchian, M.; Wang, H.; Xie, X.; McDonough, J. R.; Cui, X.; Cui, Y.;  
5 Bao, Z. *Nano Letters* **2011**, *11*, 2905.  
6 (36) Rajendra Prasad, K.; Miura, N. *Electrochemistry Communications* **2004**, *6*, 1004.  
7 (37) Horng, Y.-Y.; Lu, Y.-C.; Hsu, Y.-K.; Chen, C.-C.; Chen, L.-C.; Chen, K.-H. *Journal of Power*  
8 *Sources* **2010**, *195*, 4418.  
9 (38) Chou, S.-L.; Wang, J.-Z.; Chew, S.-Y.; Liu, H.-K.; Dou, S.-X. *Electrochemistry*  
10 *Communications* **2008**, *10*, 1724.  
11 (39) Pech, D.; Brunet, M.; Taberna, P. L.; Simon, P.; Fabre, N.; Mesnilgrete, F.; Conedera, V.;  
12 Durou, H. *Journal of Power Sources* **2010**, *195*, 1266.  
13 (40) Stoller, M. D.; Stoller, S. A.; Quarles, N.; Suk, J. W.; Murali, S.; Zhu, Y. W.; Zhu, X. J.; Ruoff,  
14 R. S. *Journal of Applied Electrochemistry* **2011**, *41*, 681.  
15 (41) Stoller, M. D.; Ruoff, R. S. *Energy & Environmental Science* **2010**, *3*, 1294.  
16 (42) Lei, Z. B.; Christov, N.; Zhao, X. S. *Energy & Environmental Science* **2011**, *4*, 1866.  
17 (43) Yan, J. A.; Khoo, E.; Sumboja, A.; Lee, P. S. *Acs Nano* **2010**, *4*, 4247.  
18 (44) Li, X.; Rong, J.; Wei, B. *ACS Nano* **2010**, *4*, 6039.  
19 (45) Cottineau, T.; Toupin, M.; Delahaye, T.; Brousse, T.; Belanger, D. *Applied Physics a-*  
20 *Materials Science & Processing* **2006**, *82*, 599.  
21 (46) Zhou, C. F.; Kumar, S.; Doyle, C. D.; Tour, J. M. *Chemistry of Materials* **2005**, *17*, 1997.  
22  
23  
24  
25  
26  
27  
28  
29  
30  
31  
32  
33  
34  
35  
36  
37  
38  
39  
40  
41  
42  
43  
44  
45  
46  
47  
48  
49  
50  
51  
52  
53  
54  
55  
56  
57  
58  
59  
60



## Figures

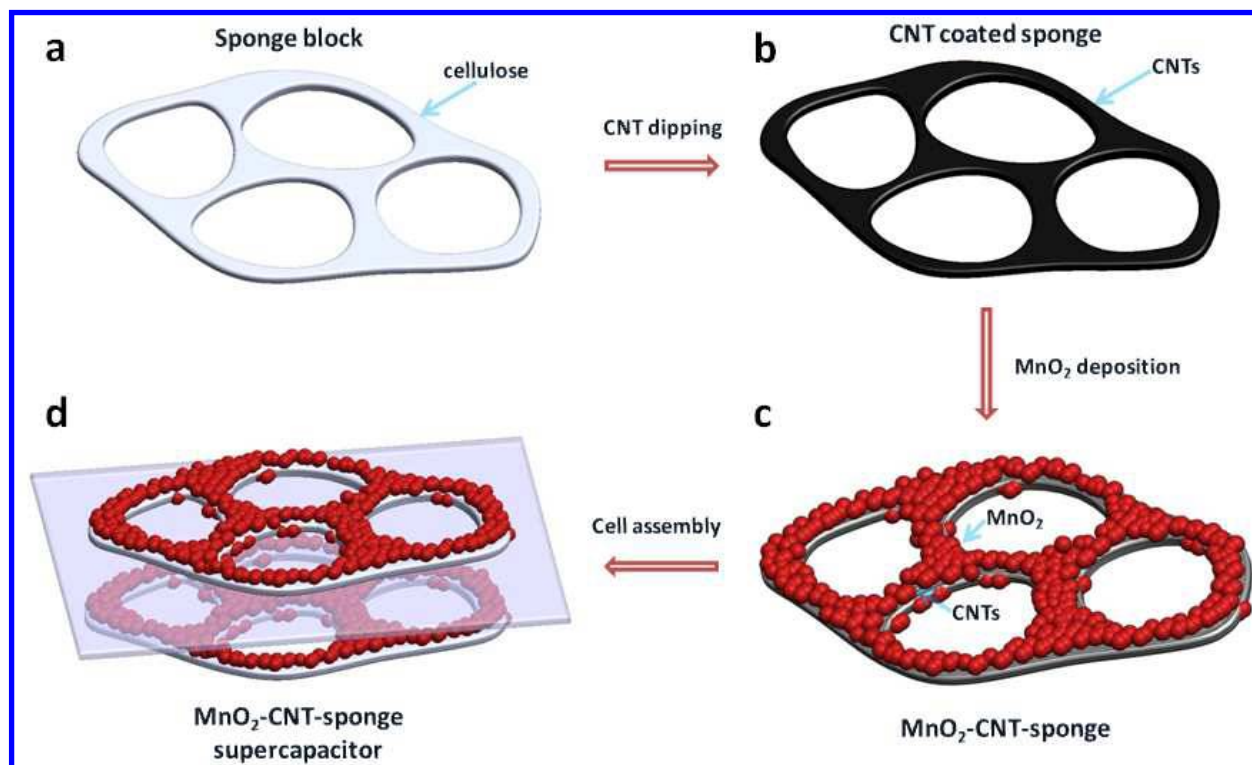


**Figure 1** Fabrication process of MnO<sub>2</sub>-CNT-sponge supercapacitors. (a) A piece of sponge is cleaned and cut into small ribbons; (b) CNTs are coated onto the skeleton of the sponge by a “dipping and drying” method; (c) Nanostructured MnO<sub>2</sub> is electrodeposited onto the conductive CNT-sponge skeleton; (d) Two pieces of MnO<sub>2</sub>-CNT-sponge electrodes were assembled into coin cell to form a MnO<sub>2</sub>-CNT-sponge supercapacitor.

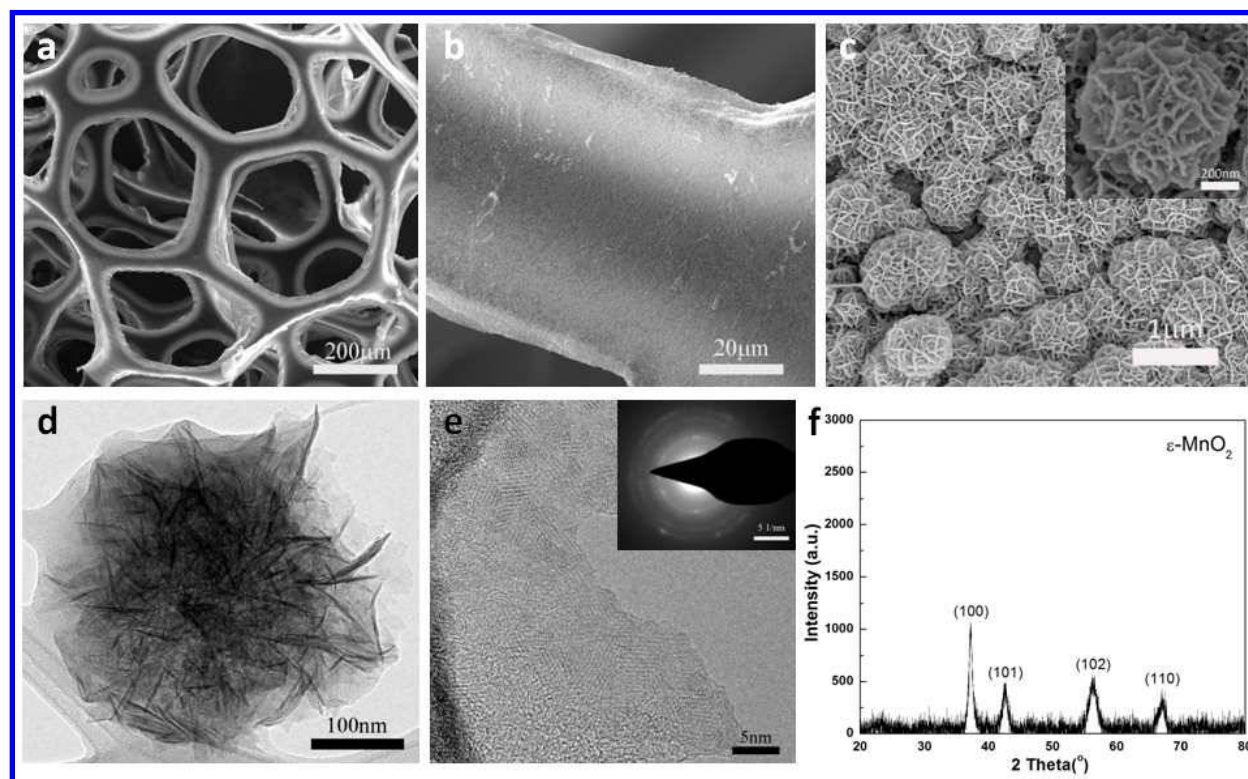


**Figure 2** Characterizations of  $\text{MnO}_2$ -CNT-sponge electrodes. a, An overall view of 3D macroporous hierarchical  $\text{MnO}_2$ -CNT-sponge electrode. b,  $\text{MnO}_2$  uniformly deposited on the skeleton of CNT-sponge. c, High magnification of porous  $\text{MnO}_2$  nanoparticles on CNT-sponge, inset shows morphology of an individual  $\text{MnO}_2$  flower-like particle. d, A TEM image of  $\text{MnO}_2$  shows highly porous structure. e, HRTEM image and the inset SAED pattern of porous  $\text{MnO}_2$  showing the polycrystalline nature of  $\text{MnO}_2$ . f, XRD of the as-synthesized structure showing the  $\epsilon$ - $\text{MnO}_2$  phase.

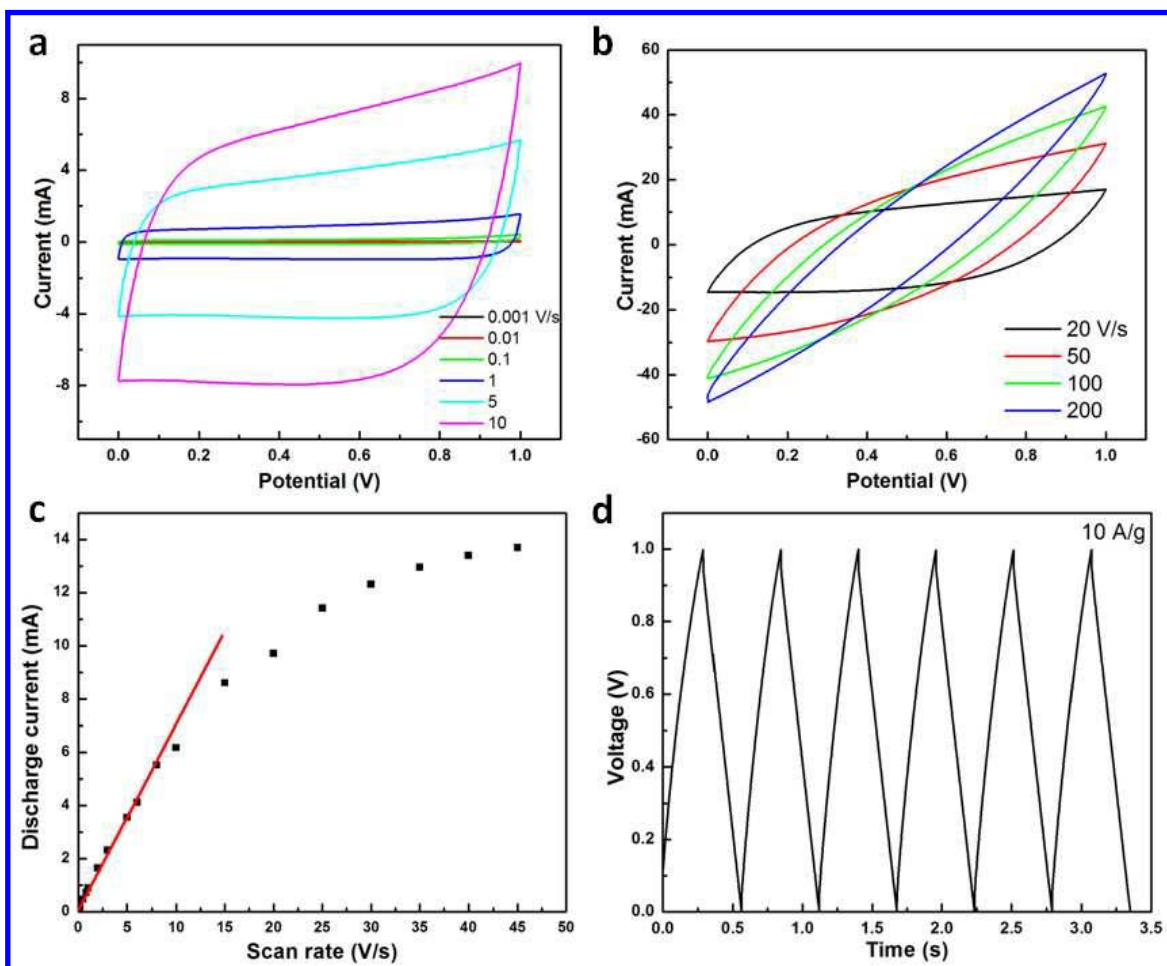


**Figure 3** Electrochemical behaviors of CNT-sponge substrates. a and b, Cyclic voltammetry scan from 1 mV/s to 10 V/s, and from 20 V/s to 200 V/s, respectively. c, Discharge currents as a function of scan rates (linear relation is obtained up to scan rate of 8 V/s). d, Galvanostatic charge-discharge curves at a specific current of 10 A/g.

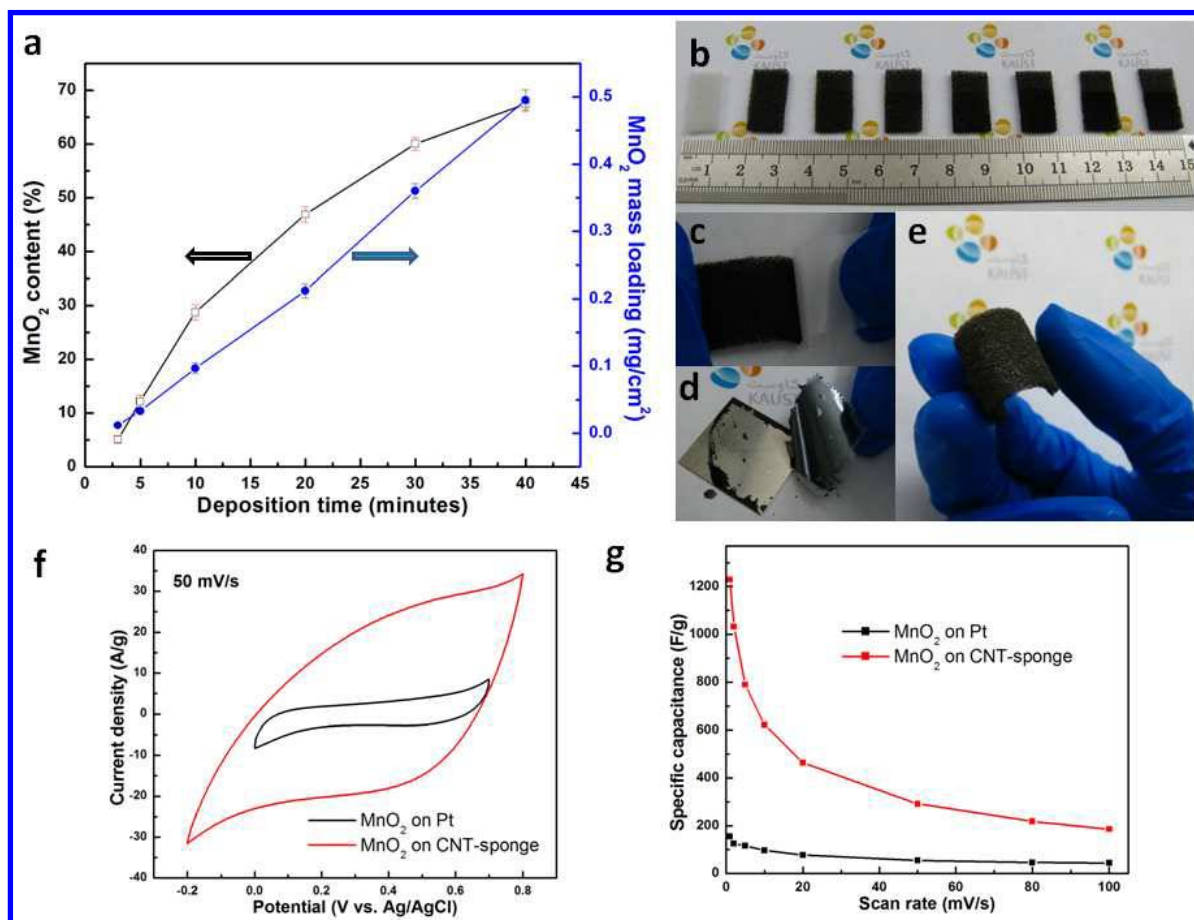


**Figure 4** MnO<sub>2</sub>-CNT-sponge supercapacitor electrodes. a, MnO<sub>2</sub> content and mass loading vs. electrodeposition time from 3 minutes to 40 minutes. b, Photograph of MnO<sub>2</sub>-CNT-sponge electrodes array, the samples from left to right are corresponding to: bare sponge, CNT-sponge, MnO<sub>2</sub> deposition on CNT-sponge for 3, 5, 10, 20, 30 and 40 minutes. c and d, Photograph of Scotch tape tests of MnO<sub>2</sub>-CNT-sponge and MnO<sub>2</sub>-Pt electrode, respectively. e, Photograph of a MnO<sub>2</sub>-CNT-sponge electrode. f, CV of MnO<sub>2</sub> on Pt vs. MnO<sub>2</sub> on CNT-sponge at 50 mV/s. g, Specific capacitance comparison between MnO<sub>2</sub>-Pt and MnO<sub>2</sub>-CNT-sponge.

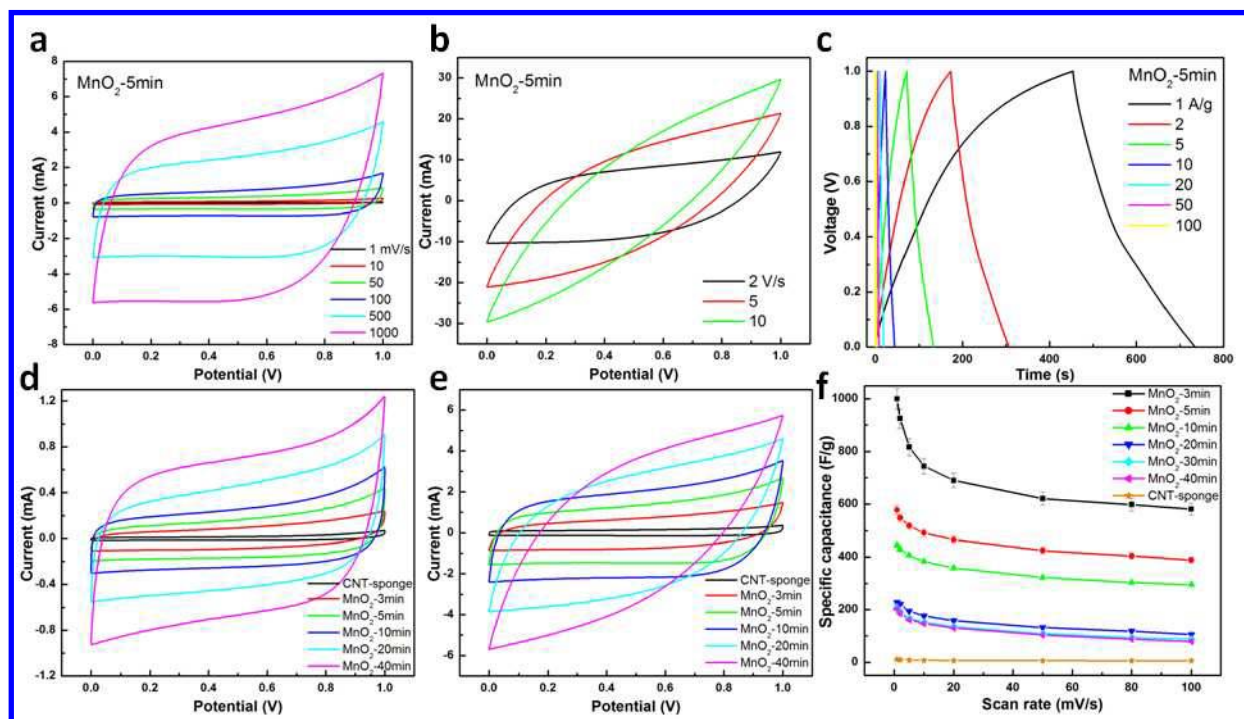


**Figure 5 Electrochemical performances of MnO<sub>2</sub>-CNT-sponge supercapacitors.** a and b, Cyclic voltammograms of a 5-minute MnO<sub>2</sub> deposition device at low and high scan rates, respectively. c, Galvanostatic charge-discharge of a 5-minute MnO<sub>2</sub> deposition device under different current densities. d and e, Cyclic voltammograms of device with different MnO<sub>2</sub> deposition times at scan rate of 20 mV/s and 200 mV/s, respectively. f, Specific capacitance versus scan rate for devices with different MnO<sub>2</sub> deposition time, ranging from 0 minute to 40 minutes. All data are taken in a 1 M Na<sub>2</sub>SO<sub>4</sub> full cell at room temperature.

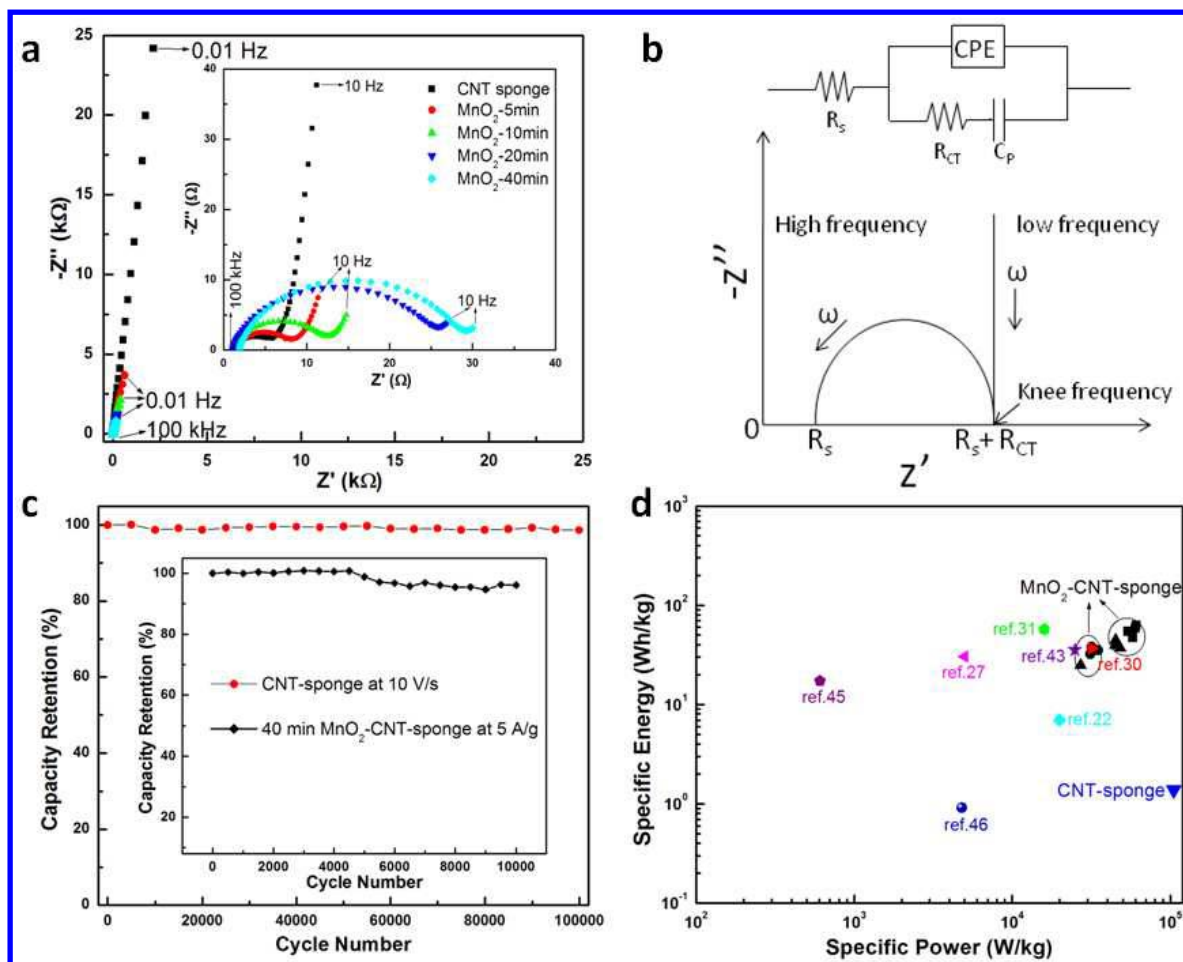


**Figure 6** Nyquist plot, equivalent circuit model, long time cycling and Ragone plot of MnO<sub>2</sub>-CNT-sponge supercapacitors. **a**, Nyquist plot of supercapacitor devices with different MnO<sub>2</sub> deposition times, ranging from 0 to 40 minutes. **b**, Equivalent circuit model of the device **c**, Capacity retention versus cycle number for CNT-sponge device up to 100,000 cycles at a high scan rate of 10 V/s and 40 minutes MnO<sub>2</sub>-CNT-sponge supercapacitors under 10,000 cycles at a specific current of 5 A/g, respectively. **d**, Ragone plot of MnO<sub>2</sub>-CNT-sponge supercapacitors and CNT-sponge devices compared with other literature.